Geoderma 446 (2024) 116903

Contents lists available at ScienceDirect

Geoderma

journal homepage: www.elsevier.com/locate/geoderma

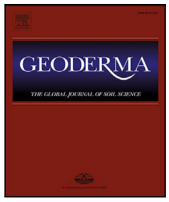

# On-site soil analysis: A novel approach combining NIR spectroscopy, remote sensing and deep learning

Michel Kok [a], Sam Sarjant [a], Sven Verweij [b], Stefan F.C. Vaessen [a], Gerard H. Ros [b,c,*]

[a] AgroCares, Nieuwe Kanaal 7, 6709 PA Wageningen, The Netherlands
[b] Nutriënten Management Instituut, Nieuwe Kanaal 7C, 6709 PA Wageningen, The Netherlands
[c] Wageningen University, Earth Systems and Global Change Group, PO Box 47, 6700 AA Wageningen, The Netherlands

ARTICLE INFO

Handling Editor: Budiman Minasny

*Keywords:*
Spectroscopy
Soil health
Carbon
Deep learning
Remote sensing
Transfer learning

ABSTRACT

Soil health is essential to global sustainable food production. Beyond its role in food production, soil also plays a crucial role in maintaining ecosystem health and mitigating climate change. Monitoring and improving the health of agricultural soils requires insight into spatial variation in soil properties and associated ecosystem functions. Measuring this variation via classic sampling and analysis on field, regional or global scale is challenging due to high spatial variability inherent to soils and to the lack of affordable and reliable measurement methods. We present here a novel and worldwide applicable approach combining NIR spectroscopy using proximal sensors, remote sensing data and deep learning models to predict the main soil properties controlling soil health in the field. These include the soil texture (clay, sand, silt), soil pH and buffered cation exchange capacity, the organic and inorganic carbon content and soil nutrient contents for nitrogen, phosphorus (P) and potassium (K). The designed model infrastructure is shown to predict all soil properties (except for P and K) on the LUCAS dataset well ($R^2 > 0.8$), and that predictive performance of field-state samples can be made comparable to lab-dried performance through transfer learning and sensor fusion with globally available covariates. These findings show that proximal soil sensing has high potential for soil health assessments and tailor-made recommendations regarding crop, soil and fertiliser management measures.

## 1. Introduction

Healthy soils provide a wide range of ecosystem services, such as the production of food, retention of nutrients, sequestration of carbon and provision of habitat. Soil health refers to the capacity of soil to function as a living ecosystem that sustains plants, animals, and humans and support ecosystem services including agricultural production (Karlen et al., 2019; Kibblewhite et al., 2008; Lal et al., 2021). Currently, agricultural soils and their provision of ecosystem services are under considerable threat due to unsustainable cultivation practices. Intensive fertilisation, tillage and mono cultures have led to negative impacts on soil biodiversity, soil acidity, soil structure and nutrient supply (Young et al., 2021). To enhance the sustainability of agriculture by management, it is key to understand the management impact on soil health and associated ecosystem services, including fertilisation strategies (Snyder et al., 2014; You et al., 2023), crop and soil management (Young et al., 2021; Busari et al., 2015). Combining these practices can minimise nutrient losses, enhance overall sustainability of agriculture, and mitigate the adverse effects of agriculture.

The implementation of sustainable soil management strategies requires a diverse set of options, each adapted to local climate, land use, yield levels, soil conditions and management opportunities (Amelung et al., 2020; You et al., 2023). This also includes a critical assessment of existing and site-specific trade-offs between ecosystem services (Lehmann et al., 2020) since soil properties and functions vary over space. Assessing these properties and functions on field and farm level requires an operational and reproducible methodology accounting for chemical, physical and biological processes and their interactions (Ros et al., 2022). Recent soil assessment frameworks like the Open Soil Index (Ros et al., 2022) and the Soil Navigator (Navigator, 2024) show that it is possible to assess soil health leveraging the existing knowledge base of agronomic research and routine laboratory data. Key soil properties include clay content, pH, soil organic carbon, and soil nutrients like nitrogen, phosphorus and potassium (Bünemann et al., 2018) given their impact on biological, chemical and physical soil processes controlling soil health (Ros, 2012; Lal, 2013; Schlatter et al., 2017; van Doorn et al., 2023). Though the assessment of these

* Corresponding author at: Wageningen University, Earth Systems and Global Change Group, PO Box 47, 6700 AA Wageningen, The Netherlands.
*E-mail address:* gerard.ros@wur.nl (G.H. Ros).

https://doi.org/10.1016/j.geoderma.2024.116903
Received 6 February 2024; Received in revised form 26 April 2024; Accepted 30 April 2024
Available online 15 May 2024

soil properties is key to monitor soil health and to take appropriate measures, their data availability is scarce since (i) classic soil sampling and analysis via wet chemistry is laborious, time consuming, and costly, and (ii) common sampling protocols ignore spatial variation occurring within and among fields. As a consequence, spatially explicit insights on soil health and management impacts at field and farm scale resolution as well as critical thresholds for associated soil functions are rare, both being crucial to guide changes in farming practices.

Sensing technologies like the use of Near-Infrared (NIR) spectroscopy may solve part of these challenges since the analysis is relatively simple, repeatable, fast and non-destructive (Reijneveld et al., 2022). The NIR soil spectra are analysed and mapped to soil properties using statistical methods or machine learning models (Barra et al., 2021). A common method for linking spectroscopy to soil wet-chemical properties is the Partial Least Squares (PLS) supervised multivariate statistical analysis technique. The PLS method is simple to implement and interpret, computationally efficient and it performs well even with small datasets. However, with a broader data space or more complex soil properties, it may not be able to explain all the subtleties of the spectral signal. A common solution is to use local PLS models (Baumann et al., 2021; Lobsey et al., 2017; Seidel et al., 2019) which find local or neighbouring samples to build a local PLS(-like) model on-the-fly and predict the sample using this local model. Although this improves modelling performance, it has some drawbacks in relation to calculation time, and the appropriate definition of neighbourhood.

Therefore, Deep Learning (DL) models have become popular due to their ability to learn abstract, hierarchical and non-linear representations of data, which overcomes the limitations of methods such as (local) PLS. These models have achieved state-of-the-art performance in various tasks such as image analysis (Yu et al., 2022; Chen et al., 2022; Wang et al., 2022), speech recognition (Zhang et al., 2020; Chung et al., 2021) and natural language processing (Brown et al., 2020). In 2019 Padarian et al. were one of the first to model soil spectroscopic data with DL. They transformed 1D spectra in 2D-spectrograms, which performed significantly better than traditional modelling like PLS. Around the same time, Riese and Keller (2019) classified soil texture using a 1D-Convolutional Neural Network (CNN). In recent years these models have become more sophisticated, introducing localisation and multiple channels (Tsakiridis et al., 2020), a combination with an Recurrent Neural Network (RNN) to address the sequential nature of spectra (Yang et al., 2020), a deeper CNN architecture (Zhong et al., 2021) and a combination with a Virtual Auto-Encoder (VAE) to generalise and simplify spectral preprocessing (Tsimpouris et al., 2021).

Where the potential of NIR has been proven for all major soil properties and some major plant nutrients, the current application to determine in-field variation of soil properties is limited by the fact that current sensors in routine agricultural laboratories are often relatively large devices unsuitable for field work, still requiring extensive soil sampling and subsequent transportation and preprocessing. Given the strong spatial variation in soil properties within and across fields, the use of portable NIR devices provide multiple advantages since they allow for in-field measurements, avoid sample preprocessing, and devices are available at low costs (Shen et al., 2022). However, portable NIR spectrometers also have several challenges in field conditions: they typically have a low spectral resolution, limited waveband range and in-field measurements come with the danger of heterogeneous sample consistency, moisture and soil presentation. Various techniques to address in-field conditions include external parameter orthogonalisation, (moisture-explicit) direct standardisation, piece-wise direct standardisation, orthogonal signal correction, and generalised least squares weighting (Zhou et al., 2021; Roudier et al., 2017; Ji et al., 2015; Minasny et al., 2011). However, each technique applies an irreversible transformation to convert the original spectral signal into a 'dry' signal. Most techniques also require local samples in the creation of the specific moisture conversion models for a local area. A benefit of deep learning is the ability to transfer models trained on one target problem over to another target problem. We hypothesise that training the model on field spectra, using transfer learning to train from a model directly trained on dry soil spectra, is an effective method to address in-field soil conditions.

In this paper we show the potential of portable near-infrared spectrometers to be used in the field worldwide to measure soil organic and inorganic carbon, clay, silt and sand content, soil pH, the CEC, and the major nutrients nitrogen, phosphorus and potassium. This significantly improves the ability to measure and monitor soil properties and soil health for both agronomic and environmental purposes. In more detail, we first evaluate an innovative DL architecture to predict the variation in aforementioned soil properties using the European LUCAS database. Second, we evaluate whether a portable NIR device can be used for direct in-field measurements using a global dataset of agricultural soils (retrieved from 36 countries) and a transfer learning method to correct for soil moisture interference in the measured spectrum. Lastly, we evaluate the value of remote sensing derived covariates for robust and reliable in-field measurements.

## 2. Material & methods

In order to test the core hypotheses of this paper, two facets of the proposed framework must be defined: the spectral, wet-chemical and remote sensing datasets used to train and evaluate model performance, and a description of the DL architecture and training procedure applied.

### 2.1. Data

Two spectra datasets are described within this paper: the LUCAS open-source VisNIR spectral dataset which contains lab-condition dry sample spectra, and the AgroCares proprietary NIR spectral dataset which contains both lab- and field-state spectra. Both datasets contain NIR spectral data and their corresponding soil wet-chemical derived properties. Furthermore, in order to test whether the inclusion of remote sensing data can improve the accuracy of proximal NIR sensors (Rossel et al., 2011) in the field, each sample in both datasets also contains the location of the sample's origin, allowing the collection of location specific covariates. A visual summary is depicted in Fig. 1.

#### 2.1.1. LUCAS

The LUCAS 2009 (Land Use/Land Cover Area Frame Survey) dataset is an open-source database that contains nearly 20,000 soil samples from 25 European countries (Tóth et al., 2013; Orgiazzi et al., 2018). The samples were collected and analysed using standardised methods in a single laboratory. Each sample was air-dried and sieved to a maximum size of 2 mm, after which their absorbance spectra were measured using a FOSS XDS Rapid Content Analyzer with wavelength 400–2500 nm at resolution 0.5 nm. The LUCAS dataset partly contains highly organic soils like peat that have an entirely different nutrient value distribution to the bulk of the dataset. To ensure metrics are not skewed, these samples are excluded from the dataset, resulting in 17,937 samples for analysis.

The LUCAS dataset contains a total of 11 wet-chemical properties, each measured within the same lab using the same procedures. These include the clay, sand and silt content (using a laser diffraction method, ISO13320:2009), the soil pH (determined in water and CaCl2, ISO10390:2005), the organic and inorganic carbon content (using dry combustion for SOC and a volumetric method for carbonates, ISO10694:1995), total *N* (using a modified Kjeldahl method, ISO11261:1995), the buffered CEC (using barium chloride extraction, ISO11260:1994), and nutrients P (P soluble in sodium hydrogen CaCO3 solution, ISO11263:1194) and K (determined via atomic absorption spectrometry after extraction with NH4OAc). Some values were measured below the limit of detection, but reported as the limit values; we have explicitly removed these for our experiments. For detailed information, see Jones et al. (2020).

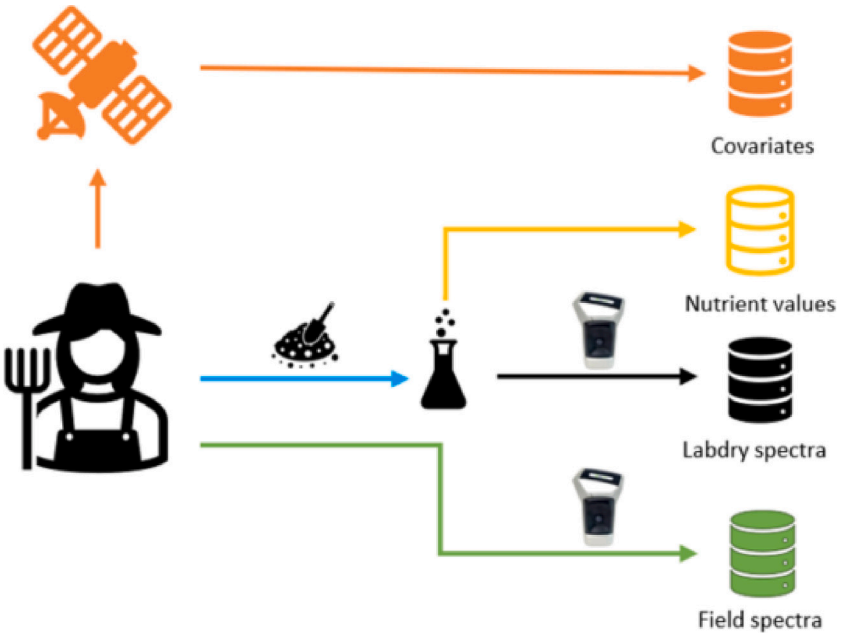


**Fig. 1.** A soil sample is scanned and collected in the field together with its GPS coordinates. The sample is sent to a laboratory for wet-chemistry analysis and re-scanned after drying and preprocessing with a NIR scanner.

*Data split.* Data was split identically to Tsakiridis et al. (2020), resulting in five training data folds. For efficiency, experiments on LUCAS were performed with a fixed validation set (fold 1).

### 2.1.2. AgroCares dataset

AgroCares has an in-house dataset of ~17,500 samples from 36 countries. These samples were analysed in the AgroCares laboratory with a variety of wet-chemical procedures for the same parameters as LUCAS. Note that although for P and K the soil extraction method is different, so the reported values are correlated to each other (Wolf and Baker, 1985), except for P when pH < 7 (Nel et al., 2023; Mallarino, 1995). Details about the laboratory methods, parameter statistics and sample locations are reported in the Appendices.

Each soil sample was air-dried, sieved and scanned with a Hand-held NIR Scanner which produces spectra with wavelength 1300–2525 nm at 5 nm resolution. Approximately 10,000 of these samples were also scanned in field-state condition before air-drying. Field-state spectra exhibit much larger moisture features and the aggregation of soil particles is likely to also obscure information that is otherwise clear in the lab-dried spectra. We refer to the lab-dried and field-state datasets as 'labdry' and 'field' respectively. Fig. 2 illustrates the differences between field and labdry spectra for the same sample. The prominent moisture peaks in field soil obscure features that are more easily observed in labdry spectra. The final spectrum used in the datasets for each sample is an averaged spectrum consisting of 2/3–5 for labdry/field sample states (as of writing, 3 scans is the current procedure for field samples). Multiple spectral measurements are to protect against the heterogeneity of the sample.

Spectral data for both labdry and field datasets were obtained using the following procedure: scanning the soil on-site, bagging the scanned soil and sending to the AgroCares laboratory, scanning the dried and sieved sample for labdry spectra and finally performing wet chemical measurements to obtain the reference values for the sample. The soil sample is collected as a composite of ten subsamples per hectare. Each subsample is taken from a 0–30 cm depth and mixed together within a bucket. For detailed instructions about scanning and sampling see AgroCares (2024) and Luebbers (2024).

*Data split.* The full dataset is split into training, validation and test sets. The training set is used to shape the weights of the DL models, while the validation set acts as a stand-in for the test set to prevent overfitting on the training data. The test set is only used to compute performance metrics and is not used for any form of (hyperparameter) optimisation or model selection. Both the validation and test sets are made with a minimum set of 60 samples per country to ensure global applicability of the models developed. The sets are defined using the following criteria:

- The properties of the soil sample are not outliers. An outlier is defined as having a value that lies 4.25 times the interquartile range outside of the soil property.
- There exists no other data point within 1 kilometer proximity.
- All target soil properties are available.
- At least 30 samples are available for this country, preferring samples that have a field scan available.

After this filtering, the 30 samples per validation and test set are collected randomly. There are 29 countries for which there are at least 60 samples (30 validation + 30 test) in the dataset making a global validation and test set of 840 samples each. Of these, 621/637 validation/test samples have a corresponding field spectrum available.

### 2.1.3. Remote sensing covariates

Both LUCAS and AgroCares datasets record GPS coordinates for every sample. These coordinates can be used to find publicly available remote sensing data about the sampling point. A total of 57 static covariates were calculated using Google Earth Engine (Gorelick et al., 2017). Elevation was selected from Multi-Error-Removed Improved-Terrain (MERIT) (Yamazaki et al., 2017) and used to calculate aspect, elevation, slope and hillshading. For Sentinel-1 the scenes recorded in 2018 to 2021 were used to calculate the Volumetric Soil Moisture (VSM) (Zakharov et al., 2020). Scenes were aggregated using median and standard deviation and grouped by season.

From Sentinel-2 the harmonised Level 2 A data from 2018 to 2021 were used to calculate Second Brightness Index (BI2) (Escadafal, 1989; Wang et al., 2021), Soil-Adjusted Total Vegetation Index (SATVI) (Marsett et al., 2006) and Transformed Vegetation Index (TVI) (Nellis and Briggs, 1992). First, the pixels in the scenes with clouds

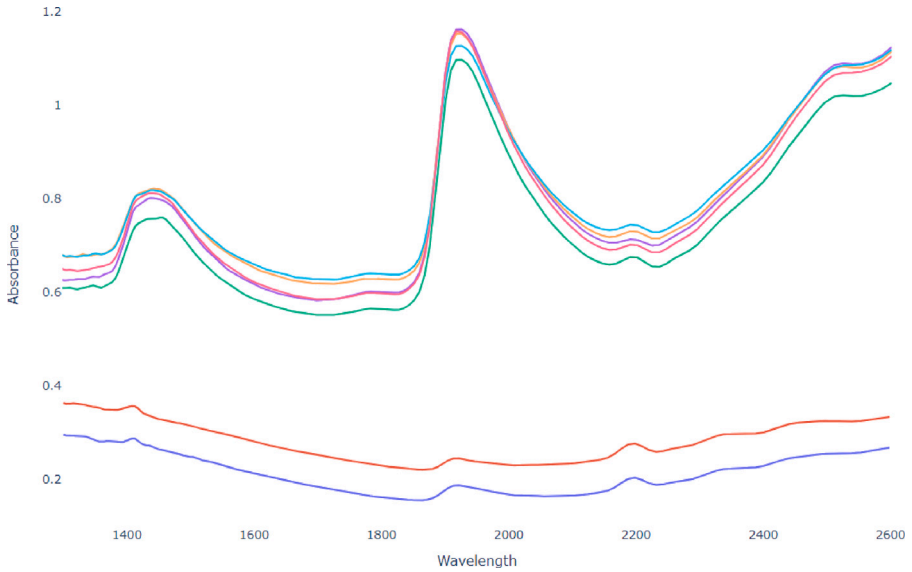


**Fig. 2.** Example of the spectral differences between 5 individual scans from a field sample (upper) and a 2 scans from a lab-dried and sieved sample (bottom).

were masked (jdbcode, 2024). For BI2 and SATVI, the scenes classified as 'bare_soil' according to band 'Scene Classification (SCL)' were selected to calculate both indices. The values were then aggregated using a median and standard deviation function. If a pixel has no scenes with a 'bare_soil' classification, the value is set to 0. The TVI was also aggregated with median and standard deviation and grouped by season.

The average predictions of bulk density, cation exchange capacity, volumetric fraction of coarse fragments, clay fraction, total nitrogen, organic carbon density, soil acidity, sand fraction, silt fraction and soil organic carbon content for the depths 0–5 cm, 5–15 cm and 15–30 cm were selected from SoilGrids 2.0 (Poggio et al., 2021). For organic carbon stocks, the average predictions from 0–30 cm were selected. To avoid data leakage from LUCAS into SoilGrids only 26 of the 57 static covariates were used for training on the LUCAS dataset.

From WorldCover, the land cover classifications from version v100 (Zanaga et al., 2021) and v200 (Zanaga et al., 2022) were selected. These categorical classifications are one-hot encoded. A full overview is given in Table 8 in the Appendices. The resulting covariates dataset for LUCAS is made publicly available at GitHub (Kok, 2024).

### 2.2. Model framework

We designed an innovative DL model framework that combines the NIR spectrum with data derived from remote sensing and the power of DL algorithms to predict the variation in a series of soil properties. A DL model, broadly speaking, consists of multiple hidden layers defined by learnable parameters that link to one-another through a series of weights and activation functions capable of capturing nonlinear complex patterns in the data. However, optimising DL models require an abundance of data and computation. The added options and flexibility of DL models also come with the drawback of many hyperparameters that need careful tuning and optimising.

A benefit of DL models is the availability of *transfer learning*, which is the ability to take a pretrained model on some domain as a starting point and exploit the learned parameters for a new domain. As highlighted earlier, in-field spectral measurements present difficulties due to moisture and sample heterogeneity, but transfer learning could allow a model to first be trained on a labdry spectral dataset before attempting to learn features from the more difficult field dataset.

The layered architecture of DL models is also flexible in terms of data flow. Data computed at one stage of the model can be reinserted later (He et al., 2015). This opens up the possibility of including multiple data sources to obtain a single prediction, for example using remote sensing data to enhance the model's predictive capabilities. Globally available datasets contain general information about a sample's location, which can be included into a model to provide a type of context alongside a sample's spectrum.

The total process of training a prediction model involves data preprocessing, model architecture definition and parameter optimisation. For all experiments, these procedures are largely the same. In all experiments we use the same convolutional neural network architecture outlined in Section 2.2.2, including remote sensing covariates when stated.

#### 2.2.1. Preprocessing

Preprocessing for spectral data typically includes two standard procedures: Savitzky–Golay (SG) smoothing (Savitzky and Golay, 1964) and the Standard Normal Variate (SNV) transformation (Dhanoa et al., 1989). Convolutional neural networks have the capability to process multiple convolutions of the same input simultaneously. So, instead of selecting specific smoothing parameters for SG followed by SNV, all combinations of window sizes (1–64) and derivatives (0–2) are applied simultaneously, to produce 192 parallel representations of every input spectrum. We also include the original unprocessed and SNV-processed versions of the input spectra to produce a total of 194 variations.

The LUCAS spectra are downsampled by a factor of ten thus leaving 420 data points per sample. Downsampling is a common operation (Tsakiridis et al., 2020; Tsimpouris et al., 2021), typically used to improve optimisation speed by reducing the number of inputs. Moreover, this step-size is consistent with the AgroCares dataset which also has a 5 nm resolution. Preliminary experiments showed no significant increase in performance when training with the highest possible resolution.

Preprocessing of each target soil parameter value involves two techniques: Box–Cox transformation (Box and Cox, 1964) to convert the data into an approximately normal distribution, followed by a rescaling transformation to rescale the Box–Cox transformed values between $[-1, 1]$. The parameters for these transformations are derived from the training dataset and applied to the validation and test sets. If remote sensing covariates are included in the experiment, they are rescaled between $[0, 1]$ without a Box–Cox transformation.

#### 2.2.2. Architecture and training procedure

The model architecture is defined as a CNN which consists of two sequential sets of convolutional layers, each followed by a normalising

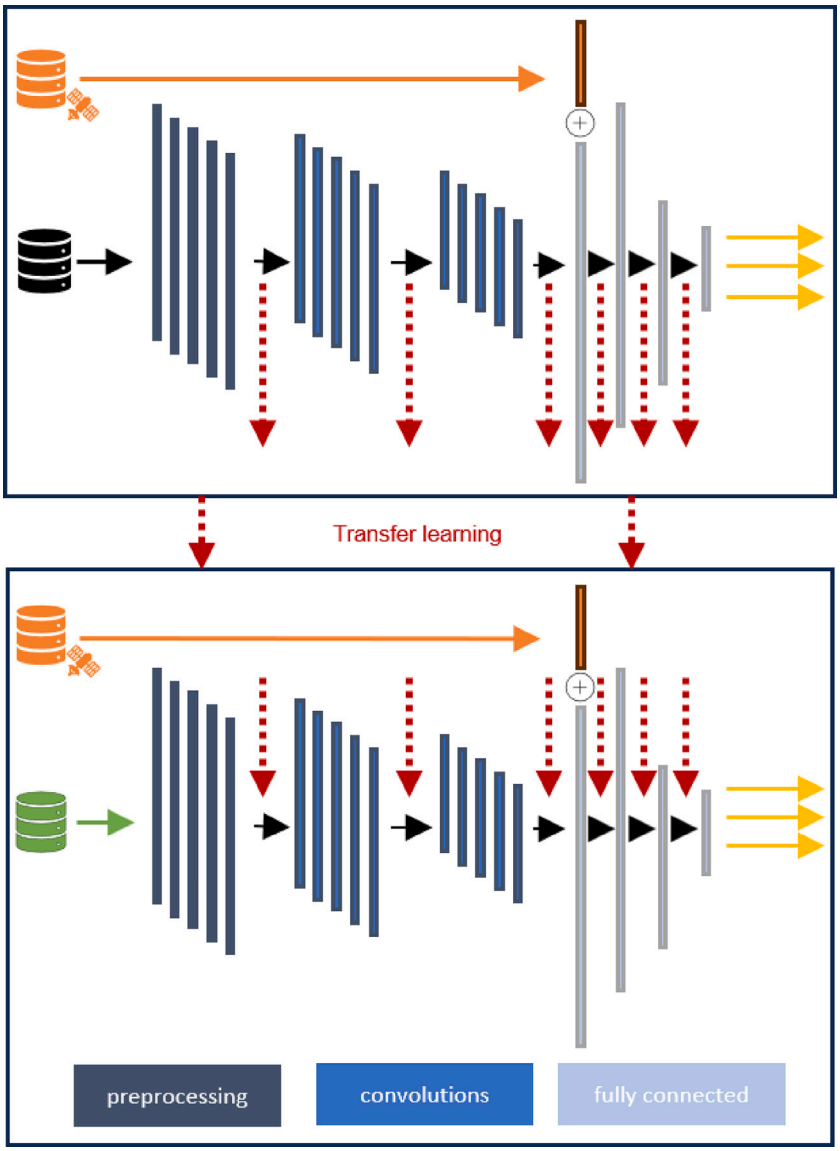


**Fig. 3.** The spectra are preprocessed, then feature maps are computed using convolutional layers which are combined in fully connected layers to obtain a final layer with $n$ predictions for $n$ targets. Optionally, remote sensing covariates are added in the final stage. Field models are constructed similarly, but they are initialised with weights from the pre-trained labdry model.

and pooling layer. The CNN is then flattened into a fully connected layer, which is concatenated with the covariate inputs if they are part of the model. This is followed by three fully connected dense layers leading into an output layer that predicts all target values simultaneously. The output layer uses the *tanh* activation function to bound the predicted values between $[-1, 1]$ (target values are rescaled as defined in Section 2.2.1). Fig. 3 illustrates the architecture visually.

While the *types* of layers used in the model are fixed, the exact hyperparameters that define each layer and the method of learning are key to producing effective models. Table 1 lists all the hyperparameters that such an architecture must use and the associated ranges of each hyperparameter.

Exhaustively optimising each hyperparameter value is computationally infeasible. To speed this up, we exploit a technique called Tree-structured Parzen Estimator (TPE) (Bergstra et al., 2011) as implemented by Optuna (Akiba et al., 2019). This algorithm optimises hyperparameter values by modelling the performance of previously sampled ranges and statistically identifying hyperparameter combinations that yield the lowest error. The error of a given combination is defined as the validation loss of the model using the hyperparameter combination. In our setup, TPE first samples seven random combinations, then starts to sample interesting combinations based on these previous results for 50 trials.

**Table 1**
Hyperparameter value ranges/choices.

| Parameter | Values |
|---|---|
| batch size | 256, 512, 1024 |
| learning rate | [1e−7, 1e−3] (logstep) |
| activation | relu, prelu, selu |
| dilation | [1, 8] (step=1) |
| kernel size | [3, 9] (step=2) |
| filters | [64, 512] (step=64) |
| neurons | [64, 512] (step=64) |
| l2 regularisation | [1e−7, 1e−3] (logstep) |
| pooling | avg, max |
| pooling size | 2, 3 |

We use the Adam optimiser (Kingma and Ba, 2014) to train for at most 500 epochs, using mean-squared error on all targets as the loss of the model. After each epoch, the loss on the validation set is also

calculated. If the validation loss does not decrease after 10 epochs the learning rate is halved, and if the validation loss does not decrease for 30 epochs the training process is terminated. The model with the best validation loss is returned as the selected model for this combination.

After hyperparameter optimisation is complete, we use an ensemble of four of the best-performing models (according to validation loss) to average test set predictions of the four models.

#### 2.2.3. Transfer learning

When training a model for predicting field spectra, transfer learning can be utilised to improve the model performance and speed of convergence. With transfer learning, features relating to soil properties can be relatively easily identified by the CNN in the labdry model, then that model forms a foundation upon which the field dataset is trained, allowing the learning process to build upon the labdry-informed features.

To perform transfer learning, the top seven training setups on the labdry dataset are selected, based on validation set loss. These each serve as a starting point of training the field dataset. Each setup is repeated three times in the same fashion as training from scratch, yielding 21 models. The reason for this repetition is to account for the instability inherent to the neural network training process. Again, the best four models (on validation set) make up the final ensemble model for field-state samples.

#### 2.2.4. Remote sensing covariates

Every sample used to train the model is linked to a spectrum (or spectra: labdry and field), target values (the measured soil properties), but also the geographic location from where the sample originated. Remote sensing covariates are obtained by querying publicly available remote sensing data sources based on GPS coordinates (see Section 2.1.3 for details). These features are not powerful enough alone to predict soil properties accurately, but rather they should be treated as contextual information alongside the spectral signal. When covariates are included in the model architecture, they are provided as an additional input to the model, preprocessed (Section 2.2.1) and concatenated beside the features obtained after the convolutional blocks.

#### 2.2.5. Evaluation metrics

We primarily use the metrics $R^2$ (coefficient of determination) and $RPIQ$ (ratio of performance to interquartile distance) to evaluate the performance of the DL models and describe the variation in measured soil properties. For all results, an independent test set is used to produce impartial results. The $RPIQ$ is used instead of $RMSE$ (root mean squared error) because the latter is dependent on the range of the observed values whereas $RPIQ$ is given relative to the range of the target values, so it can be compared across target values originating from different datasets. For bias we report mean error $ME$ to evaluate under/overprediction.

Given a dataset of $n$ samples, ground truth $y$ and prediction $\hat{y}$, the metrics can be calculated as follows:

$$R^2(y,\hat{y}) = 1 - \frac{\sum_{i=1}^{n}(y_i-\hat{y}_i)^2}{\sum_{i=1}^{n}(y_i-\bar{y}_i)^2} \tag{1}$$

$$RMSE(y,\hat{y}) = \sqrt{\frac{\sum_{i=1}^{n}(y_i-\hat{y}_i)^2}{n}} \tag{2}$$

$$RPIQ(y,\hat{y}) = \frac{Q_3-Q_1}{RMSE(y,\hat{y})} \tag{3}$$

$$ME(y,\hat{y}) = \frac{\sum_{i=1}^{n}(y_i-\hat{y}_i)}{n} \tag{4}$$

with $Q_1$ and $Q_3$ being the 25% and 75% quartile of the test set reference data respectively.

## 3. Results and discussion

### 3.1. Prediction of soil properties on dried soils

The designed DL infrastructure and calibration procedure made it possible to predict the majority of the soil properties with a high accuracy (Table 2). The best predictions were found for pH and CaCO3 with an $R^2 > 0.92$. Contents of clay, sand, soil organic carbon and total nitrogen could also be predicted with $R^2$ values above 0.8 and $RPIQ$ values almost above 3.0. The variation in soil phosphorus and potassium is more challenging to predict given $R^2$ values between 0.4 and 0.6. Alternative state-of-the-art modelling approaches (Tsimpouris et al., 2021; Tsakiridis et al., 2020) being tested on LUCAS dataset show very comparable performance to the approach tested in this study for all soil properties. There are other modelling approaches being evaluated on the LUCAS dataset (Padarian et al., 2019; Zhong et al., 2021), but these typically include the small set of highly organic samples which tend to skew the evaluation metrics due to the extreme values included. We have included the full set of soil properties in our models, as their inclusion has shown no negative effect on the performance of the other properties in experiments.

Measuring this set of soil properties with high precision and accuracy (Table 2) allows one to assess soil health for a series of chemical, physical and biological soil functions as shown by Bünemann et al. (2018) who reviewed existing soil properties and indicators being used in soil quality assessments. For example, Ros et al. (2022) derived more than 21 soil indicators to assess soil health with respect to sustainable crop production. The performance of the proximal sensor predictions show that the soil nutrient supply for nitrogen and potassium as well the pH buffering can be evaluated in view of crop and soil type dependent thresholds. The performance for phosphorus is currently too low for appropriate underpinning of fertiliser recommendations and can likely only be used to distinguish P deficient from P rich soils. Similarly, the moisture retention capacity, the aggregate stability, erodibility, workability, and sealing risk can be derived since clay content, sand content and soil organic carbon are known. Ease of sampling and measurement are often considered one of the major requirements for soil quality indicators, and reliability and costs are also considered important.

Using global models for local applications could be problematic because they usually capture general trends about the data, at the cost of local performances. However, DL models have the flexibility and capacity to characterise problems into many features without compromising local specificity. Alternatives like spiking or local models suffer from increased computational demands and complexity, both in terms of how to handle locality or similarity of samples and how to maintain potentially many models for a global application. Our DL approach can be seen as a natural extension of the algorithm developed by Tsakiridis et al. (2020) but it significantly differs from Tsimpouris et al. (2021), who use a separate, densely stacked auto-encoder instead of the convolutional layers and bootstrap aggregation (bagging) as a form of ensembling. Our models improve over Tsakiridis et al. (2020), which can be explained by the use of extensive preprocessing, a broader range of learnable parameters and performing additional hyperparameter tuning. However, our model approach typically performs somewhat worse than Tsimpouris et al. (2021) (Table 2). Possible explanations for the lower performance could be that they did not remove values below the limit of detection or that their ensembling procedure is much more extensive as it requires 50 separate models to be built and individually optimised.

The preprocessing steps (i.e. Savitzky–Golay derivative smoothing) have been argued as unnecessary (Ng et al., 2019, 2020) since convolutional filters were found to construct filters that resemble common preprocessing techniques from the raw spectrum. However, we found the preprocessing improves the mean $R^2$ and $RPIQ$ by 3% and 6% respectively on the LUCAS dataset (no covariates). Our hypothesis is

**Table 2**
State-of-the-Art comparison. See Eqs. (1)–(4) for metric definitions. $ME$ and some elements are not found in Tsimpouris et al. (2021). CaCO3 statistics from Tsimpouris et al. appear to be on a different range and hence are excluded.

| Element | Tsimpouris et al. | | | Ours | | | |
|---|---|---|---|---|---|---|---|
| | $R^2$ | $RPIQ$ | $RMSE$ | $R^2$ | $RPIQ$ | $RMSE$ | $ME$ |
| clay | 0.88 | 4.15 | 4.32 | 0.87 | 3.85 | 4.68 | 0.21 |
| silt | 0.80 | 3.19 | 8.14 | 0.78 | 2.96 | 8.79 | 0.58 |
| sand | 0.84 | 4.34 | 10.36 | 0.82 | 4.00 | 11.25 | 0.27 |
| pH (H2O) | 0.93 | 7.08 | 0.33 | 0.92 | 6.34 | 0.37 | 0.00 |
| OC | 0.88 | 2.29 | 9.96 | 0.81 | 2.38 | 8.48 | 0.88 |
| N | 0.86 | 2.34 | 0.59 | 0.81 | 2.42 | 0.54 | 0.05 |
| CEC | 0.85 | 2.94 | 3.93 | 0.84 | 3.04 | 3.74 | 0.31 |
| Mean | 0.86 | 3.76 | 5.38 | 0.84 | 3.57 | 5.41 | 0.33 |
| pH (CaCl2) | | *missing* | | 0.93 | 6.97 | 0.37 | 0.00 |
| P | | *missing* | | 0.35 | 1.38 | 23.16 | 4.19 |
| K | | *missing* | | 0.52 | 1.14 | 147.09 | 17.84 |
| CaCO3 | | *excluded* | | 0.94 | 3.08 | 37.71 | 0.90 |

**Table 3**
AgroCares NIR-dataset performances for combinations of sample state, use of transfer and use of covariates. Sample state $L$ = labdry spectra model, $F$ = field spectra model and $F_L$ = field spectra model transferred from labdry model. See Eqs. (1)–(4) for metric definitions. $RMSE$ and $ME$ can be found in Table 7 in Appendices.

| Covariates | Without | | | | | | With | | | | | |
|---|---|---|---|---|---|---|---|---|---|---|---|---|
| Metric | $R^2$ | | | $RPIQ$ | | | $R^2$ | | | $RPIQ$ | | |
| Sample state | $L$ | $F$ | $F_L$ | $L$ | $F$ | $F_L$ | $L$ | $F$ | $F_L$ | $L$ | $F$ | $F_L$ |
| Experiment | (a) | (b) | (c) | (a) | (b) | (c) | (d) | (e) | (f) | (d) | (e) | (f) |
| clay | 0.70 | 0.67 | 0.69 | 2.70 | 2.64 | 2.70 | 0.71 | 0.67 | 0.68 | 2.77 | 2.62 | 2.66 |
| silt | 0.68 | 0.59 | 0.59 | 2.92 | 2.54 | 2.54 | 0.73 | 0.62 | 0.67 | 3.18 | 2.65 | 2.85 |
| sand | 0.69 | 0.63 | 0.64 | 3.17 | 2.94 | 2.96 | 0.73 | 0.68 | 0.73 | 3.41 | 3.18 | 3.43 |
| pH (KCl) | 0.74 | 0.61 | 0.63 | 3.59 | 2.99 | 3.08 | 0.76 | 0.68 | 0.70 | 3.75 | 3.27 | 3.42 |
| pH (H2O) | 0.75 | 0.64 | 0.66 | 3.18 | 2.68 | 2.74 | 0.77 | 0.69 | 0.71 | 3.30 | 2.88 | 2.97 |
| OC | 0.83 | 0.78 | 0.79 | 1.77 | 1.60 | 1.61 | 0.87 | 0.80 | 0.80 | 2.03 | 1.68 | 1.66 |
| N | 0.79 | 0.77 | 0.78 | 1.72 | 1.70 | 1.74 | 0.83 | 0.72 | 0.77 | 1.88 | 1.55 | 1.72 |
| CEC | 0.81 | 0.79 | 0.79 | 2.86 | 2.71 | 2.69 | 0.83 | 0.79 | 0.80 | 3.00 | 2.71 | 2.80 |
| P | 0.51 | 0.46 | 0.44 | 1.15 | 1.32 | 1.30 | 0.59 | 0.49 | 0.52 | 1.26 | 1.33 | 1.37 |
| K | 0.44 | 0.37 | 0.34 | 1.32 | 1.21 | 1.18 | 0.48 | 0.38 | 0.39 | 1.37 | 1.21 | 1.22 |
| Mean | 0.69 | 0.63 | 0.64 | 2.44 | 2.23 | 2.25 | 0.73 | 0.65 | 0.68 | 2.60 | 2.31 | 2.41 |

that by removing this step, the CNN is better able to focus on feature extraction during training. It is not known how much each of the 194 preprocessing channels individually contributes to performance at this time, and the influence of preprocessing algorithms warrants further study.

### 3.2. Prediction of soil properties under field conditions

While most studies in relation to NIR sensors focus on spectra collected in controlled conditions, the use of mobile sensors in the field is a challenge since NIR reflectance is sensitive to variation in environmental conditions, in particular soil moisture (Bünemann et al., 2018). To assess whether NIR can be used as a monitoring tool directly on field-state samples, the performance of the field-state model was evaluated and compared to performance of the labdry (dried and ground) model using the AgroCares NIR-dataset. The performance of field-state models was compared under two conditions: one situation where the model was built 'from scratch' directly on field-state spectral data, and another one where the model was built on top of a previously-built labdry-state model via transfer learning.

Moisture obfuscates the light's interaction with the sample and is therefore a source of noise which makes moist samples more difficult to predict. The effect of moisture on model performance can be clearly seen in Table 3 with labdry ($a$) and field soils ($b$). On average, $R^2$ and $RPIQ$ drop by 9.5% and 9.4% respectively when building a model from field soil directly. Exploiting the labdry dataset by using transfer learning to train the field model ($c$) from the labdry model yields a small average benefit over direct field training ($b$), but when also including covariates (experiments ($d$), ($e$) and ($f$), see Section 3.3 for more details), the improvement gained from transfer learning increases more substantially.

The transfer learning approach as applied in our study is simple to apply, but it requires that both air-dried and field-moist spectra are available for each sample. Additional tests where the same soil was rewetted at various moisture contents showed that the transfer learning approach was applicable across a wide range of moisture levels (data not shown). Only at high moisture contents (above field capacity) there is a slight decrease in the prediction performance. Reflecting on the model performance for all soil properties, each model is guaranteed to be on par (e.g. organic carbon) or better in terms of performance on both $R^2$ and $RPIQ$ metrics (P and K are exceptions when not using covariates). When labdry models are already available, this has the additional benefit that a transfer learning field model is much faster to converge than training a model from scratch which saves training costs.

For all elements except arguably P and K the model can be used to get a good estimate of the nutrients in the soil which enables regular soil health monitoring. Even for the worst element, low potassium regions in the field will still be discernible from a high potassium portion. This implies that the use of proximal sensing in the field can help farmers to optimise their soil management while accounting for spatial variation in soil properties and associated threats, functions or

**Table 4**
Covariate performance (excluding SoilGrids) on the LUCAS dataset. See Eqs. (1)–(4) for metric definitions.

| Covariates | Without | | With | |
|---|---|---|---|---|
| Element | $R^2$ | $RPIQ$ | $R^2$ | $RPIQ$ |
| clay | 0.85 | 3.67 | 0.86 | 3.73 |
| silt | 0.74 | 2.76 | 0.75 | 2.83 |
| sand | 0.79 | 3.73 | 0.80 | 3.81 |
| pH.in.CaCl2 | 0.93 | 6.89 | 0.93 | 7.03 |
| pH.in.H2O | 0.92 | 6.29 | 0.92 | 6.42 |
| OC | 0.83 | 1.92 | 0.85 | 2.01 |
| N | 0.81 | 1.99 | 0.82 | 2.07 |
| CEC | 0.82 | 2.64 | 0.82 | 2.70 |
| P | 0.27 | 1.15 | 0.26 | 1.15 |
| K | 0.44 | 1.02 | 0.48 | 1.06 |
| CaCO3 | 0.94 | 2.76 | 0.93 | 2.69 |
| Mean | 0.76 | 3.17 | 0.77 | 3.23 |

ecosystem services. It has also the potential to improve the agronomic knowledge base that has been derived from field averaged values thereby ignoring the spatial variation within fields (Ros et al., 2022).

The earlier extensive review of Bünemann et al. (2018) describes three main limitations of spectroscopic techniques when applied in the field. First, sensors determine only the properties of the first millimeters of the soil area analysed. Second, soil moisture levels, particle density and roughness of the soil surface can affect the predicted soil properties. Lastly, the accuracy and precision is strongly controlled by the calibration and validation process and the prediction is as good as the calibration data set. Our study shows that all three aspects can be covered by well designed and automated procedures for sampling, field analysis, model selection and calibration. Even under field conditions around 70% to 80% of the variation in soil properties (except for P and K) can be explained with the DL model.

### 3.3. Leveraging remote sensing data for sensor accuracy

Remote sensing techniques provide a powerful means for characterisation and monitoring of near-surface soil properties and land use changes at reasonable temporal and spatial resolutions. Conceptually, McBratney et al. (2003) came with the so-called SCORPAN approach to analyse their influence on soil formation, a framework to predict the spatial variation in soil properties based on soil forming factors, like climate, land use, organisms, relief, parent material, time and spatial position. Since the major soil properties like SOC, clay content and pH are for a large extent affected by parent material, geohydrology and the position in the landscape, one might expect that fusing handheld spectra with remote sensing data will improve the accuracy and precision of estimated soil properties (Asgari et al., 2020; Grunwald et al., 2015).

For the LUCAS dataset (Table 4) there is a small performance improvement when adding (non-SoilGrids) covariates. On the AgroCares dataset (Table 3), the inclusion of the SoilGrids covariates results in a more pronounced improvement. The AgroCares labdry dataset improved by an average 5.7% and 7.0% on $R^2$ and $RPIQ$ respectively. On field-transferred spectra the average increase was in a similar range with 8.0% and 6.1%. Figs. 4 and 5 illustrate performances across labdry, field, and field with transfer, all using covariates. The increased performance is consistent across all soil properties with the strongest effect on the weakest nutrient $P$.

For almost all soil properties the sensor fusing in a single model improved the prediction. Similar findings have been presented for yield maps (Dobermann and Ping, 2004), farm based mapping of carbon stocks (van der Voort et al., 2023) implying that fusion of sensor sets with available soil-environmental databases provide promising pathways for soil assessments facilitating decision making to adapt soil and crop management in view of complex local, regional and global environmental challenges.

Since the use of remote sensing data in field-state models for proximal mobile sensors produces performances that are almost at the same level as models that are built on labdry and ground spectra alone, we conclude that remote sensing derived covariates can be used as compensation for the moisture artefacts that remain in a field sample even after transfer learning models are being applied. However, it is important to note that the application in the field also becomes dependent on this data and is more sensitive to the cited accuracy of the sampling location. Since a broad spectrum of soil information has already been adopted in precision farming systems to optimise decisions, data availability is not necessarily a limiting factor in large areas in the world.

In order to understand the contributions of each of the covariates used, a simple feature permutation analysis was performed. The following procedure was repeated ten times on the AgroCares field dataset: within the test set, for each covariate, the order of the covariates were randomly permuted across all samples, producing new output prediction values for every sample in the test set. The absolute differences in predictions from the non-permuted predictions were then summed for every target value, producing a relative ranking of importance in how much the value of a covariate affects the predictions. Attribution values for all covariates can be found in Table 8 in the Appendix. Covariates related to texture, seasonal VSM, and landcover classifications were found to be most important. These align with the SCORPAN approach in that these properties are informative for soil form, climate, and land use. It is important to realise that attribution is not necessarily causation as there can be many solutions for a given problem (Kirkpatrick et al., 2017). This is one of the reasons eXplainable Artificial Intelligence (XAI) is challenging and still an active research area (Ali et al., 2023). An extensive covariate importance analysis is therefore left for future work.

Note that this paper focuses on main chemical and physical soil properties controlling agronomic and environmental soil functioning thereby ignoring soil biological measurements (Bünemann et al., 2018; Lehmann et al., 2020). Due to the strong relationship of soil biological processes with soil organic matter, pH, texture and nutrient levels (Reijneveld et al., 2022), soil sensors might nevertheless provide insights in the temporal and spatial dynamics of soil functions controlled by soil biology. Similarly, measurements of labile, reactive or stable carbon fractions (Ghani et al., 2003; Haynes, 2005; Ros, 2012) might add value to the total SOC being used in this study.

## 4. Conclusion

Portable near-infrared spectrometers can be used to determine soil properties relevant for soil quality assessments in the field, allowing farmers and land users to monitor soil health indicators over space and time, and to adapt crop, soil and fertiliser management to the local situation. The chosen DL model architecture and calibration and validation procedures applied allowed the development of robust and accurate model predictions for a series of agronomic relevant soil properties. These include the soil texture, the organic and inorganic C content, the soil pH and buffered cation exchange capacity as well as the total nitrogen content. Applying transfer learning made it possible to correct for variations in soil moisture, ensuring high accuracy on in situ measurements done in the field. Sensor fusion with remote sensor data showed clear improvements for most of the soil properties included, implying that the use of spatial explicit covariates will enhance the predictive power of soil-spectral prediction models.

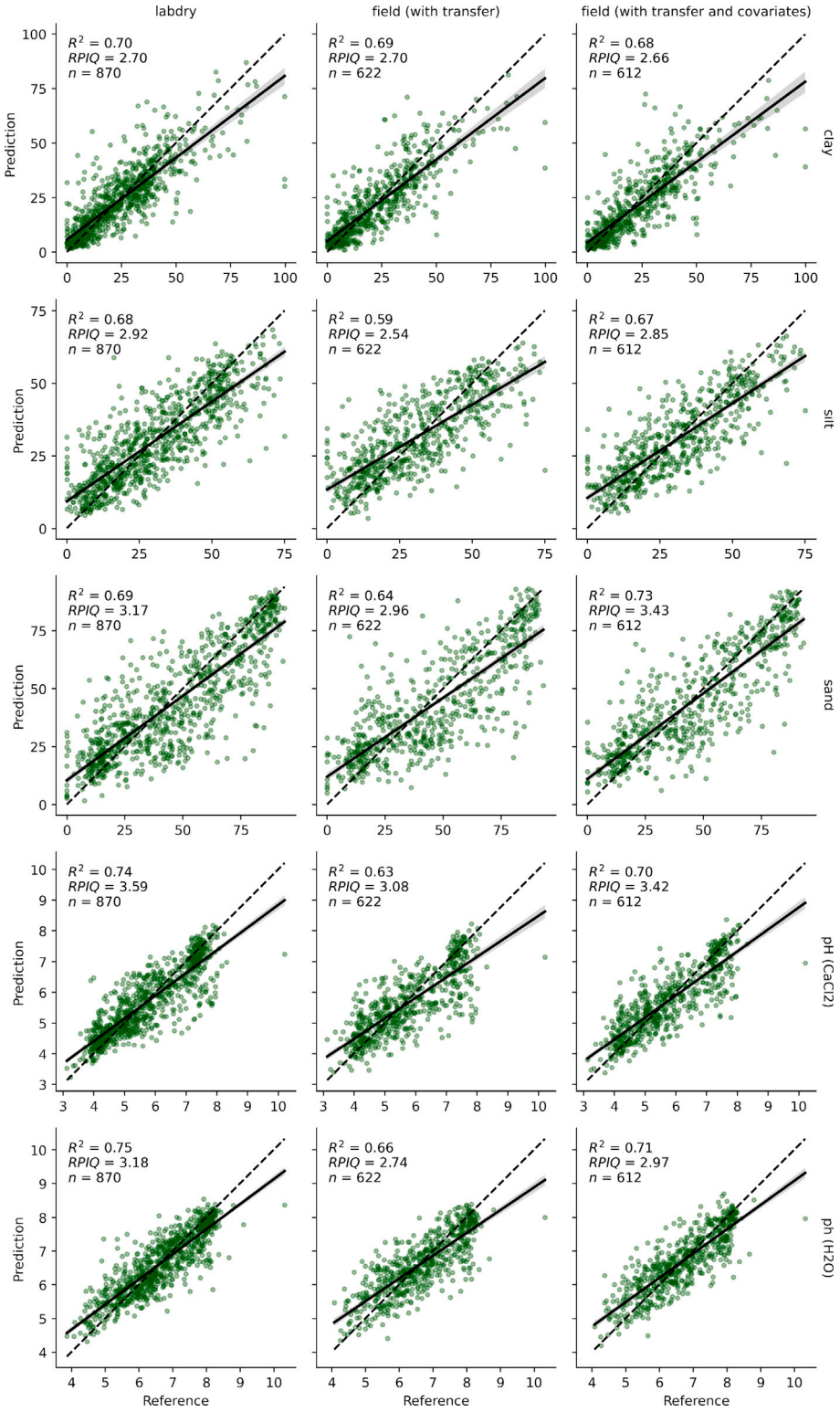


**Fig. 4.** Test set prediction results clay, silt, sand and pH (from top to bottom) for labdry (left) and field samples without (middle) and including (right) remote sensing covariates.

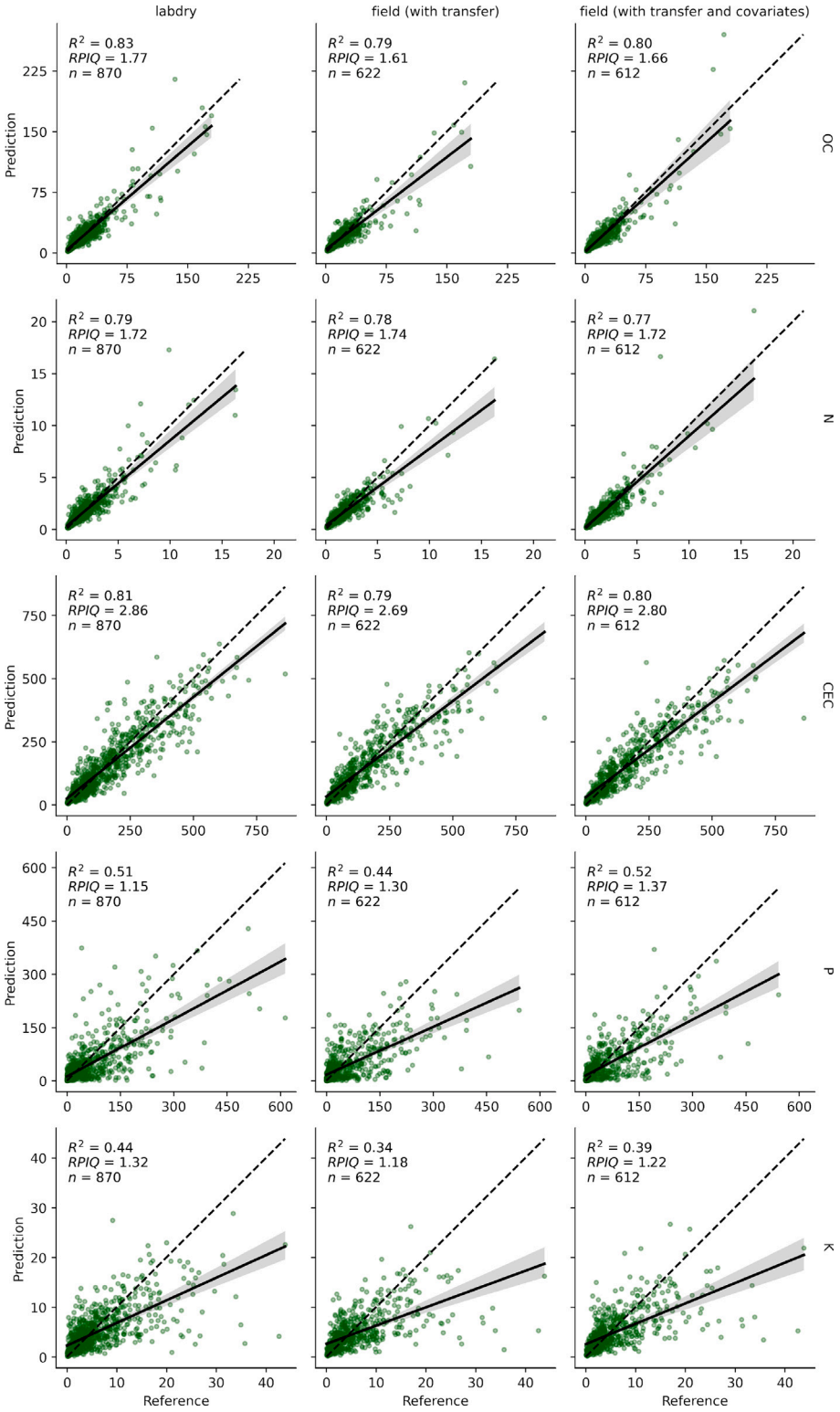


**Fig. 5.** Test set prediction results for OC, N, CEC, P and K (from top to bottom) for labdry (left) and field samples without (middle) and including (right) remote sensing covariates.

## CRediT authorship contribution statement

**Michel Kok:** Writing – original draft, Visualization, Validation, Software, Resources, Project administration, Methodology, Investigation, Formal analysis, Data curation, Conceptualization. **Sam Sarjant:** Writing – review & editing, Validation, Software, Resources, Methodology, Investigation, Formal analysis, Data curation, Conceptualization. **Sven Verweij:** Writing – review & editing, Resources, Methodology, Data curation, Conceptualization. **Stefan F.C. Vaessen:** Writing – review & editing, Supervision, Conceptualization. **Gerard H. Ros:** Writing – review & editing, Supervision, Methodology, Conceptualization.

## Declaration of competing interest

The authors declare the following financial interests/personal relationships which may be considered as potential competing interests: Michel Kok reports financial support was provided by AgroCares. Sam Sarjant reports financial support was provided by AgroCares. Sven Verweij reports financial support was provided by Nutriënten Management Instituut. Stefan Vaessen reports financial support was provided by AgroCares. Gerard Ros reports financial support was provided by Nutriënten Management Instituut. If there are other authors, they declare that they have no known competing financial interests or personal relationships that could have appeared to influence the work reported in this paper.

## Data availability

Data will be made available on request.

## Appendix A. Supplementary data

Supplementary material related to this article can be found online at https://doi.org/10.1016/j.geoderma.2024.116903.

## References


AgroCares, 2024. Getting started series E. https://support.soilcares.com/hc/en-us/sections/360000098434-Getting-started-Series-E. (Online; Accessed 24 April 2024).

Akiba, T., Sano, S., Yanase, T., Ohta, T., Koyama, M., 2019. Optuna: A next-generation hyperparameter optimization framework. In: Proceedings of the 25rd International Conference on Knowledge Discovery and Data Mining. pp. 1–10, arXiv:1907.10902.

Ali, S., Abuhmed, T., El-Sappagh, S., Muhammad, K., Alonso-Moral, J.M., Confalonieri, R., Guidotti, R., Del Ser, J., Díaz-Rodríguez, N., Herrera, F., 2023. Explainable artificial intelligence (XAI): What we know and what is left to attain Trustworthy Artificial Intelligence. Inf. Fusion 99, 101805.

Amelung, W., Bossio, D., de Vries, W., Kögel-Knabner, I., Lehmann, J., Amundson, R., Bol, R., Collins, C., Lal, R., Leifeld, J., et al., 2020. Towards a global-scale soil climate mitigation strategy. Nature Commun. 11 (1), 5427.

Asgari, N., Ayoubi, S., Jafari, A., Demattê, J.A., 2020. Incorporating environmental variables, remote and proximal sensing data for digital soil mapping of USDA soil great groups. Int. J. Remote Sens. 41 (19), 7624–7648.

Barra, I., Haefele, S.M., Sakrabani, R., Kebede, F., 2021. Soil spectroscopy with the use of chemometrics, machine learning and pre-processing techniques in soil diagnosis: Recent advances–A review. TRAC Trends Anal. Chem. 135, 116166.

Baumann, P., Helfenstein, A., Gubler, A., Keller, A., Meuli, R.G., Wächter, D., Lee, J., Viscarra Rossel, R., Six, J., 2021. Developing the swiss soil spectral library for local estimation and monitoring. Soil Discuss. 2021, 1–32.

Bergstra, J., Bardenet, R., Bengio, Y., Kégl, B., 2011. Algorithms for hyper-parameter optimization. In: Proceedings of the 24th International Conference on Neural Information Processing Systems. NIPS '11, Curran Associates Inc., Red Hook, NY, USA, pp. 2546–2554.

Box, G.E., Cox, D.R., 1964. An analysis of transformations. J. R. Stat. Soc. Ser. B Stat. Methodol. 26 (2), 211–243.

Brown, T.B., Mann, B., Ryder, N., Subbiah, M., Kaplan, J., Dhariwal, P., Neelakantan, A., Shyam, P., Sastry, G., Askell, A., Agarwal, S., Herbert-Voss, A., Krueger, G., Henighan, T., Child, R., Ramesh, A., Ziegler, D.M., Wu, J., Winter, C., Hesse, C., Chen, M., Sigler, E., Litwin, M., Gray, S., Chess, B., Clark, J., Berner, C., McCandlish, S., Radford, A., Sutskever, I., Amodei, D., 2020. Language models are few-shot learners. CoRR abs/2005.14165. URL: https://arxiv.org/abs/2005.14165.

Bünemann, E.K., Bongiorno, G., Bai, Z., Creamer, R.E., De Deyn, G., De Goede, R., Fleskens, L., Geissen, V., Kuyper, T.W., Mäder, P., et al., 2018. Soil quality–A critical review. Soil Biol. Biochem. 120, 105–125.

Busari, M.A., Kukal, S.S., Kaur, A., Bhatt, R., Dulazi, A.A., 2015. Conservation tillage impacts on soil, crop and the environment. Int. Soil Water Conserv. Res. 3 (2), 119–129.

Chen, Z., Duan, Y., Wang, W., He, J., Lu, T., Dai, J., Qiao, Y., 2022. Vision transformer adapter for dense predictions. http://dx.doi.org/10.48550/ARXIV.2205.08534, URL: https://arxiv.org/abs/2205.08534.

Chung, Y.A., Zhang, Y., Han, W., Chiu, C.C., Qin, J., Pang, R., Wu, Y., 2021. W2v-BERT: Combining contrastive learning and masked language modeling for self-supervised speech pre-training. http://dx.doi.org/10.48550/ARXIV.2108.06209, URL: https://arxiv.org/abs/2108.06209.

Dhanoa, M.S., Lister, S.J., Barnes, R.J., 1989. Standard normal variate transformation and de-trending of near-infrared diffuse reflectance spectra. Appl. Spectrosc. 43 (5), 772–777, https://opg.optica.org/abstract.cfm?uri=as-43-5-772 https://opg.optica.org/as/abstract.cfm?uri=as-43-5-772.

Dobermann, A., Ping, J., 2004. Geostatistical integration of yield monitor data and remote sensing improves yield maps. Agron. J. 96 (1), 285–297.

Escadafal, R., 1989. Remote sensing of arid soil surface color with Landsat thematic mapper. Adv. Space Res. 9 (1), 159–163. http://dx.doi.org/10.1016/0273-1177(89)90481-X, URL: https://www.sciencedirect.com/science/article/pii/027311778990481X.

Ghani, A., Dexter, M., Perrott, K., 2003. Hot-water extractable carbon in soils: a sensitive measurement for determining impacts of fertilisation, grazing and cultivation. Soil Biol. Biochem. 35 (9), 1231–1243.

Gorelick, N., Hancher, M., Dixon, M., Ilyushchenko, S., Thau, D., Moore, R., 2017. Google Earth Engine: Planetary-scale geospatial analysis for everyone. Remote Sens. Environ. 202, 18–27. http://dx.doi.org/10.1016/j.rse.2017.06.031, URL: https://linkinghub.elsevier.com/retrieve/pii/S0034425717302900.

Grunwald, S., Vasques, G.M., Rivero, R.G., 2015. Fusion of soil and remote sensing data to model soil properties. Adv. Agron. 131, 1–109.

Haynes, R., 2005. Labile organic matter fractions as central components of the quality of agricultural soils: anoverview. Adv. Agron. 5, 221–268.

He, K., Zhang, X., Ren, S., Sun, J., 2015. Deep residual learning for image recognition. CoRR abs/1512.03385. URL: http://arxiv.org/abs/1512.03385.

jdbcode, 2024. Sentinel-2 cloud masking. https://developers.google.com/earth-engine/tutorials/community/sentinel-2-s2cloudless. (Online; Accessed 24 April 2024).

Ji, W., Viscarra Rossel, R., Shi, Z., 2015. Improved estimates of organic carbon using proximally sensed vis-NIR spectra corrected by piecewise direct standardization. Eur. J. Soil Sci. 66 (4), 670–678.

Jones, A., Fernandez-Ugalde, O., Scarpa, S., 2020. LUCAS 2015 topsoil survey. Presentation of dataset and results, EUR 30332 EN, publications office of the European union: Luxembourg. 10, 616084, JRC121325.

Karlen, D.L., Veum, K.S., Sudduth, K.A., Obrycki, J.F., Nunes, M.R., 2019. Soil health assessment: Past accomplishments, current activities, and future opportunities. Soil Tillage Res. 195, 104365.

Kibblewhite, M., Ritz, K., Swift, M., 2008. Soil health in agricultural systems. Philos. Trans. R. Soc. B 363 (1492), 685–701.

Kingma, D.P., Ba, J., 2014. Adam: A method for stochastic optimization. http://dx.doi.org/10.48550/ARXIV.1412.6980, URL: https://arxiv.org/abs/1412.6980.

Kirkpatrick, J., Pascanu, R., Rabinowitz, N., Veness, J., Desjardins, G., Rusu, A.A., Milan, K., Quan, J., Ramalho, T., Grabska-Barwinska, A., et al., 2017. Overcoming catastrophic forgetting in neural networks. Proc. Natl. Acad. Sci. 114 (13), 3521–3526.

Kok, M., 2024. LUCAS covariates. https://github.com/AgroCares/lucas_covariates. (Online; Accessed 24 April 2024).

Lal, R., 2013. Intensive agriculture and the soil carbon pool. J. Crop Improv. 27 (6), 735–751.

Lal, R., Bouma, J., Brevik, E., Dawson, L., Field, D.J., Glaser, B., Hatano, R., Hartemink, A.E., Kosaki, T., Lascelles, B., et al., 2021. Soils and sustainable development goals of the united nations: An international union of soil sciences perspective. Geoderma Reg. 25, e00398.

Lehmann, J., Bossio, D.A., Kögel-Knabner, I., Rillig, M.C., 2020. The concept and future prospects of soil health. Nat. Rev. Earth Environ. 1 (10), 544–553. http://dx.doi.org/10.1038/s43017-020-0080-8.

Lobsey, C., Viscarra Rossel, R., Roudier, P., Hedley, C., 2017. Rs-local data-mines information from spectral libraries to improve local calibrations. Eur. J. Soil Sci. 68 (6), 840–852.

Luebbers, T., 2024. Soil sampling. https://support.soilcares.com/hc/en-us/articles/115002127945-Soil-sampling. (Online; Accessed 24 April 2024).

Mallarino, A., 1995. Comparison of mehlich-3, olsen, and bray-P1 procedures for phosphorus in calcareous soils. In: The 25th North Central Extension-Industry Soil Fertility Conference. St. Louis, Missouri, pp. 96–101.

Marsett, R.C., Qi, J., Heilman, P., Biedenbender, S.H., Carolyn Watson, M., Amer, S., Weltz, M., Goodrich, D., Marsett, R., 2006. Remote sensing for grassland management in the arid southwest. Rangel. Ecol. Manage. 59 (5), 530–540. http://dx.doi.org/10.2111/05-201R.1, URL: https://www.sciencedirect.com/science/article/pii/S1550742406500600.

McBratney, A.B., Santos, M.M., Minasny, B., 2003. On digital soil mapping. Geoderma 117 (1–2), 3–52.

Minasny, B., McBratney, A.B., Bellon-Maurel, V., Roger, J.M., Gobrecht, A., Ferrand, L., Joalland, S., 2011. Removing the effect of soil moisture from NIR diffuse reflectance spectra for the prediction of soil organic carbon. Geoderma 167, 118–124.

Navigator, S., 2024. Soil navigator. http://www.soilnavigator.eu/. (Online; Accessed 24 April 2024).

Nel, T., Bruneel, Y., Smolders, E., 2023. Comparison of five methods to determine the cation exchange capacity of soil. J. Plant Nutr. Soil Sci. 186 (3), 311–320. http://dx.doi.org/10.1002/jpln.202200378, URL: https://onlinelibrary.wiley.com/doi/abs/10.1002/jpln.202200378.

Nellis, M.D., Briggs, J.M., 1992. Transformed vegetation index for measuring spatial variation in drought impacted biomass on Konza Prairie, Kansas. Trans. Kansas Acad. Sci. (1903-) 95 (1/2), 93–99. http://dx.doi.org/10.2307/3628024, URL: https://www.jstor.org/stable/3628024. Publisher: Kansas Academy of Science.

Ng, W., Minasny, B., Mendes, W.d., Demattê, J.A.M., 2020. The influence of training sample size on the accuracy of deep learning models for the prediction of soil properties with near-infrared spectroscopy data. Soil 6 (2), 565–578.

Ng, W., Minasny, B., Montazerolghaem, M., Padarian, J., Ferguson, R., Bailey, S., McBratney, A.B., 2019. Convolutional neural network for simultaneous prediction of several soil properties using visible/near-infrared, mid-infrared, and their combined spectra. Geoderma 352, 251–267.

Orgiazzi, A., Ballabio, C., Panagos, P., Jones, A., Fernández-Ugalde, O., 2018. LUCAS soil, the largest expandable soil dataset for Europe: a review. Eur. J. Soil Sci. 69 (1), 140–153. http://dx.doi.org/10.1111/ejss.12499, URL: https://bsssjournals.onlinelibrary.wiley.com/doi/abs/10.1111/ejss.12499.

Padarian, J., Minasny, B., McBratney, A., 2019. Using deep learning to predict soil properties from regional spectral data. Geoderma Reg. 16, e00198. http://dx.doi.org/10.1016/j.geodrs.2018.e00198, URL: https://www.sciencedirect.com/science/article/pii/S2352009418302785.

Poggio, L., de Sousa, L.M., Batjes, N.H., Heuvelink, G.B.M., Kempen, B., Ribeiro, E., Rossiter, D., 2021. SoilGrids 2.0: producing soil information for the globe with quantified spatial uncertainty. SOIL 7 (1), 217–240. http://dx.doi.org/10.5194/soil-7-217-2021, URL: https://soil.copernicus.org/articles/7/217/2021/. Publisher: Copernicus GmbH.

Reijneveld, J.A., van Oostrum, M.J., Brolsma, K.M., Fletcher, D., Oenema, O., 2022. Empower innovations in routine soil testing. Agronomy 12 (1), 191.

Riese, F.M., Keller, S., 2019. Soil texture classification with 1d convolutional neural networks based on hyperspectral data. ISPRS Ann. Photogramm. Remote Sens. Spatial Inf. Sci. IV-2/W5, 615–621. http://dx.doi.org/10.5194/isprs-annals-IV-2-W5-615-2019, URL: https://www.isprs-ann-photogramm-remote-sens-spatial-inf-sci.net/IV-2-W5/615/2019/.

Ros, G.H., 2012. Predicting soil N mineralization using organic matter fractions and soil properties: A re-analysis of literature data. Soil Biol. Biochem. 45, 132–135.

Ros, G.H., Verweij, S.E., Janssen, S.J., De Haan, J., Fujita, Y., 2022. An open soil health assessment framework facilitating sustainable soil management. Environ. Sci. Technol. 56 (23), 17375–17384.

Rossel, R.V., Adamchuk, V., Sudduth, K., McKenzie, N., Lobsey, C., 2011. Proximal soil sensing: An effective approach for soil measurements in space and time. Adv. Agron. 113, 243–291.

Roudier, P., Hedley, C., Lobsey, C., Rossel, R.V., Leroux, C., 2017. Evaluation of two methods to eliminate the effect of water from soil vis-NIR spectra for predictions of organic carbon. Geoderma 296, 98–107.

Savitzky, A., Golay, M.J., 1964. Smoothing and differentiation of data by simplified least squares procedures. Anal. Chem. 36, 1627–1639. http://dx.doi.org/10.1021/AC60214A047/ASSET/AC60214A047.FP.PNG_V03, URL: https://pubs.acs.org/doi/abs/10.1021/ac60214a047.

Schlatter, D., Kinkel, L., Thomashow, L., Weller, D., Paulitz, T., 2017. Disease suppressive soils: new insights from the soil microbiome. Phytopathology 107 (11), 1284–1297.

Seidel, M., Hutengs, C., Ludwig, B., Thiele-Bruhn, S., Vohland, M., 2019. Strategies for the efficient estimation of soil organic carbon at the field scale with vis-NIR spectroscopy: Spectral libraries and spiking vs. local calibrations. Geoderma 354, 113856.

Shen, Z., D'Agui, H., Walden, L., Zhang, M., Yiu, T.M., Dixon, K., Nevill, P., Cross, A., Matangulu, M., Hu, Y., Viscarra Rossel, R.A., 2022. Miniaturised visible and near-infrared spectrometers for assessing soil health indicators in mine site rehabilitation. SOIL 8 (2), 467–486. http://dx.doi.org/10.5194/soil-8-467-2022, URL: https://soil.copernicus.org/articles/8/467/2022/.

Snyder, C., Davidson, E., Smith, P., Venterea, R., 2014. Agriculture: sustainable crop and animal production to help mitigate nitrous oxide emissions. Curr. Opin. Environ. Sustain. 9, 46–54.

Tóth, G., Jones, A., Montanarella, L., 2013. The LUCAS topsoil database and derived information on the regional variability of cropland topsoil properties in the European Union. Environ. Monit. Assess. 185 (9), 7409–7425.

Tsakiridis, N.L., Keramaris, K.D., Theocharis, J.B., Zalidis, G.C., 2020. Simultaneous prediction of soil properties from VNIR-SWIR spectra using a localized multi-channel 1-D convolutional neural network. Geoderma 367, http://dx.doi.org/10.1016/J.GEODERMA.2020.114208.

Tsimpouris, E., Tsakiridis, N.L., Theocharis, J.B., 2021. Using autoencoders to compress soil VNIR–SWIR spectra for more robust prediction of soil properties. Geoderma 393, 114967. http://dx.doi.org/10.1016/j.geoderma.2021.114967, URL: https://www.sciencedirect.com/science/article/pii/S0016706121000410.

van der Voort, T.S., Verweij, S., Fujita, Y., Ros, G.H., 2023. Enabling soil carbon farming: presentation of a robust, affordable, and scalable method for soil carbon stock assessment. Agron. Sustain. Dev. 43 (1), 22.

van Doorn, M., van Rotterdam, D., Ros, G., Koopmans, G.F., Smolders, E., de Vries, W., 2023. The phosphorus saturation degree as a universal agronomic and environmental soil P test. Crit. Rev. Environ. Sci. Technol. 1–20.

Wang, W., Dai, J., Chen, Z., Huang, Z., Li, Z., Zhu, X., Hu, X., Lu, T., Lu, L., Li, H., Wang, X., Qiao, Y., 2022. InternImage: Exploring large-scale vision foundation models with deformable convolutions. http://dx.doi.org/10.48550/ARXIV.2211.05778, URL: https://arxiv.org/abs/2211.05778.

Wang, K., Qi, Y., Guo, W., Zhang, J., Chang, Q., 2021. Retrieval and mapping of soil organic carbon using sentinel-2A spectral images from bare cropland in autumn. Remote Sens. 13 (6), 1072. http://dx.doi.org/10.3390/rs13061072, URL: https://www.mdpi.com/2072-4292/13/6/1072. Number: 6 Publisher: Multidisciplinary Digital Publishing Institute.

Wolf, A.M., Baker, D., 1985. Comparisons of soil test phosphorus by Olsen, Bray P1, Mehlich I and Mehlich III methods. Commun. Soil Sci. Plant Anal. 16 (5), 467–484.

Yamazaki, D., Ikeshima, D., Tawatari, R., Yamaguchi, T., O'Loughlin, F., Neal, J.C., Sampson, C.C., Kanae, S., Bates, P.D., 2017. A high-accuracy map of global terrain elevations. Geophys. Res. Lett. 44 (11), 5844–5853. http://dx.doi.org/10.1002/2017GL072874, URL: https://onlinelibrary.wiley.com/doi/abs/10.1002/2017GL072874.

Yang, J., Wang, X., Wang, R., Wang, H., 2020. Combination of convolutional neural networks and recurrent neural networks for predicting soil properties using Vis–NIR spectroscopy. Geoderma 380, 114616. http://dx.doi.org/10.1016/j.geoderma.2020.114616, URL: https://www.sciencedirect.com/science/article/pii/S0016706120301415.

You, L., Ros, G.H., Chen, Y., Shao, Q., Young, M.D., Zhang, F., de Vries, W., 2023. Global mean nitrogen recovery efficiency in croplands can be enhanced by optimal nutrient, crop and soil management practices. Nature Commun. 14 (1), 5747.

Young, M.D., Ros, G.H., de Vries, W., 2021. Impacts of agronomic measures on crop, soil, and environmental indicators: A review and synthesis of meta-analysis. Agric. Ecosyst. Environ. 319, 107551.

Yu, J., Wang, Z., Vasudevan, V., Yeung, L., Seyedhosseini, M., Wu, Y., 2022. CoCa: Contrastive captioners are image-text foundation models. http://dx.doi.org/10.48550/ARXIV.2205.01917, URL: https://arxiv.org/abs/2205.01917.

Zakharov, I., Kapfer, M., Hornung, J., Kohlsmith, S., Puestow, T., Howell, M., Henschel, M.D., 2020. Retrieval of surface soil moisture from Sentinel-1 time series for reclamation of wetland sites. IEEE J. Sel. Top. Appl. Earth Obs. Remote Sens. 13, 3569–3578. http://dx.doi.org/10.1109/JSTARS.2020.3004062, URL: https://ieeexplore.ieee.org/document/9122451. Conference Name: IEEE Journal of Selected Topics in Applied Earth Observations and Remote Sensing.

Zanaga, D., Van De Kerchove, R., Daems, D., De Keersmaecker, W., Brockmann, C., Kirches, G., Wevers, J., Cartus, O., Santoro, M., Fritz, S., Lesiv, M., Herold, M., Tsendbazar, N.E., Xu, P., Ramoino, F., Arino, O., 2022. ESA WorldCover 10 m 2021 v200. http://dx.doi.org/10.5281/ZENODO.7254221, URL: https://zenodo.org/record/7254221.

Zanaga, D., Van De Kerchove, R., De Keersmaecker, W., Souverijns, N., Brockmann, C., Quast, R., Wevers, J., Grosu, A., Paccini, A., Vergnaud, S., Cartus, O., Santoro, M., Fritz, S., Georgieva, I., Lesiv, M., Carter, S., Herold, M., Li, L., Tsendbazar, N.E., Ramoino, F., Arino, O., 2021. ESA WorldCover 10 m 2020 v100. http://dx.doi.org/10.5281/ZENODO.5571936, URL: https://zenodo.org/record/5571936.

Zhang, Y., Qin, J., Park, D.S., Han, W., Chiu, C.C., Pang, R., Le, Q.V., Wu, Y., 2020. Pushing the limits of semi-supervised learning for automatic speech recognition. http://dx.doi.org/10.48550/ARXIV.2010.10504, URL: https://arxiv.org/abs/2010.10504.

Zhong, L., Guo, X., Xu, Z., Ding, M., 2021. Soil properties: Their prediction and feature extraction from the LUCAS spectral library using deep convolutional neural networks. Geoderma 402, 115366. http://dx.doi.org/10.1016/j.geoderma.2021.115366, URL: https://www.sciencedirect.com/science/article/pii/S0016706121004468.

Zhou, P., Yang, W., Li, M., Wang, W., 2021. A new coupled elimination method of soil moisture and particle size interferences on predicting soil total nitrogen concentration through discrete NIR spectral band data. Remote Sens. 13 (4), 762.